Geospatial modelling reveals flood-driven inequities in nutrition-sensitive healthcare access across Kampala, Uganda

Rik Lubbers

r.u.lubbers@rug.nl

University Medical Center Groningen https://orcid.org/0000-0002-2772-1524

Gerd Weitkamp

Fleur Hierink

GeoHealth group, Institute for Environmental Sciences & Institute of Global Health, University of Geneva
https://orcid.org/0000-0002-2727-0540

Nicolas Ray

GeoHealth group, Institute for Environmental Sciences & Institute of Global Health, University of Geneva
https://orcid.org/0000-0002-4696-5313

Frederick Oporia

Otto Businge

https://orcid.org/0000-0001-8216-8859

Regien Biesma

Article

Keywords:

Posted Date: December 3rd, 2025

DOI: https://doi.org/10.21203/rs.3.rs-8055572/v1

Additional Declarations: There is **NO** Competing Interest.

Geospatial modelling reveals flood-driven inequities in nutrition-sensitive healthcare access across Kampala, Uganda

Rik U. Lubbers (MSc) [1, 2]*, Gerd Weitkamp (PhD) [2], Fleur Hierink (PhD) [3, 4], Nicolas Ray (PhD) [3, 4], Frederick Oporia (PhD) [5], Otto Businge (MSc) [5], and Regien Biesma (PhD) [1, 6]

1 Global Health Unit, Department of Health Sciences, University Medical Centre Groningen, Groningen, the Netherlands

2 Department of Cultural Geography, Faculty of Spatial Sciences, University of Groningen, Groningen, the Netherlands

3 GeoHealth group, Institute of Global Health, Faculty of Medicine, University of Geneva. 9 Chemin des Mines, 1202 Geneva, Switzerland.

4 Institute for Environmental Sciences, University of Geneva. Boulevard Carl-Vogt 66, 1205 Geneva, Switzerland.

5 Department of Disease Control and Environmental Health, Makerere University School of Public Health, Uganda.

6 Department of Global Public Health and Bioethics, Julius Center for Health Sciences and Primary Care, University Medical Center Utrecht

* Corresponding author: Rik U. Lubbers, Global Health Unit, Department of Health Sciences, University Medical Centre Groningen, Antonius Deusinglaan 1, 9713 AV Groningen, The Netherlands, r.u.lubbers@umcg.nl

Abstract

Background

Urban floods slow or sever travel to healthcare facilities, reducing timely access to maternal and child healthcare in Kampala. We estimated flood-related changes in walking access to all public and private-not-for-profit facilities and to hospitals.

Methods

We modelled walking travel times at ~10 m resolution using land cover, roads, hydrography, and elevation, treating water bodies as barriers except at mapped crossings. Speeds reflected adults with young children, with wet-surface penalties and depth rules. We simulated 15 rainfall scenarios, 20–100 mm over 1, 3, or 6 hours, and computed anisotropic travel time to the nearest facility. Outcomes were parish-level, population-weighted changes from baseline, stratified by a maternal, child, and socioeconomic vulnerability index.

Results

Here we show travel time increased across all scenarios. City-wide means to the nearest facility ranged from 11.2 minutes at 20 mm over 6 hours to 19.1 minutes at 100 mm over 1 hour. For hospitals, means ranged from 23.0 to 55.8 minutes. At fixed rainfall, shorter storms produced larger increases than longer storms with the same depth. Under the 100 mm, 1 hour scenario, variation across vulnerability levels was modest for all facilities, 23.5 versus 21.8 minutes between highest and lowest quartiles, but substantial for hospitals, 97.6 versus 43.1 minutes.

Conclusions

Floods limit walking access in Kampala, with the largest penalties for hospital care and in high-vulnerability parishes. These delays risk undermining timely antenatal and postnatal care, child illness assessment, and immunisation contacts, routine moments through which supplementation, growth monitoring, and caregiver counselling are delivered.

Plain language summary:

Floods can make it harder for caregivers with young children to reach clinics and hospitals. We studied Kampala, Uganda, to estimate how floods change walking time to healthcare. We combined maps of land, roads, water, and elevation with realistic walking speeds on wet surfaces and tested fifteen flood situations, from lighter, longer storms to intense, short ones. Here we show that travel times increased in every case: up to about 19 minutes to the nearest clinic and 56 minutes to the nearest hospital for the most intense one-hour storms. Delays were greatest in high-vulnerability neighbourhoods and outer areas, while central areas changed less. These results can guide service placement.

Introduction

Floods are the most common extreme weather event globally and are expected to intensify due to climate change [1,2]. In low and middle income countries, particularly rapidly urbanising cities, flood risk is amplified by unregulated construction, extensive impermeable surfaces, and inadequate drainage infrastructure [3–5]. These conditions increase the likelihood and severity of urban floods, which in turn can cause systemic disruptions across sectors, including transportation, food systems, and healthcare [6–8].

Strengthening healthcare accessibility under such conditions is critical for building resilient, equitable health systems that are responsive to climate threats and social inequalities [9–11]. For maternal, newborn and child health (MNCH), these shocks matter not only for direct injuries, infections, or childbirth-related emergencies, but also because they interrupt essential primary healthcare and nutrition-sensitive delivery pathways. A nutrition-sensitive lens does not measure nutrition outcomes directly, such as diet quality or malnutrition rates, but instead examines how another sector, in this case healthcare accessibility, affects nutrition-related determinants like maternal and child health services, food security, and the capacity to deliver nutrition interventions during climate shocks [12–14]. These delivery opportunities include antenatal care (ANC), postnatal care (PNC), sick-child consultations, and immunisation contacts, where supplementation, growth monitoring, and caregiver counselling occur [15,16]. Moreover, undernutrition and infection form a self-reinforcing cycle [17], and floods raise undernutrition risk [18,19], therefore maintaining MNCH access during flood shocks is intrinsically nutrition sensitive.

Access to healthcare during and after floods depends not only on whether facilities remain functional but also on geographical accessibility, the time and distance required to reach them. Limited geographical accessibility is a critical barrier in health-seeking behaviour and is consistently associated with delayed or foregone care [20–22]. When floods slow travel or sever links, delays can cascade from first contact to referral, shrinking the window for effective treatment of infectious diseases [9].

In urban settings, floods may obstruct mobility by reducing travel speed and rendering entire road segments impassable. In dense urban networks, small capacity losses can produce large travel-time

penalties; because congestion is nonlinear, disruptions to a few critical links propagate across catchments, forcing long and costly detours that disproportionately burden low-income caregivers [23,24]. Studies from Jakarta, Accra, and Lagos show that floods disrupt road networks, create disconnected urban subregions, and disproportionately affect low-income settlements, increasing travel times and reducing geographical access to healthcare [23,25,26].

Kampala, Uganda's capital, offers a compelling case study of these risks. Rapid urbanization and expansion into flood-prone valleys and wetlands, coupled with incomplete drainage, leave large low-lying neighbourhoods exposed to pluvial flooding [3,5,27–31]. City risk assessments and flood models show that even short-duration rainfall events can generate significant disruptions and increase travel times [32]. These mobility shocks interact with gendered and socioeconomic constraints: many low-income caregivers rely on walking or informal paratransit, face safety and cost barriers, and must prioritize caregiving and income-earning responsibilities that magnify the impact of even modest additional travel time [33–36].

Although urban flood impacts on mobility are documented in diverse settings, the evidence base linking floods to geographical access to nutrition-sensitive delivery platforms in rapidly growing African cities remains thin and fragmented [10]. Yet few analyses are vulnerability-disaggregated, nutrition-sensitive, and intra-urban in focus. For Kampala, prior quantitative work examined hospital access under a return-period flood [32], but did not assess non-hospital MNCH service points, did not differentiate impacts by maternal or child vulnerability, and did not test multiple short, intense storm typologies typical of the city. More broadly, a recent scoping review finds that evidence on extreme weather and maternal health in LMICs under-represents urban, access-focused studies and rarely quantifies intra-city inequalities [36]. This gap constrains planners' capacity to safeguard the nutrition-sensitive delivery pathway, ANC, PNC, sick-child care, and immunisation, through which supplementation, growth monitoring, and counselling are delivered [12,15,16], underscoring the need for spatially resolved evidence to guide resilient service planning.

This study addresses that gap by quantifying flood-induced changes in geographical accessibility to public and private-not-for-profit (PNFP) facilities across Kampala under 15 rainfall–

duration scenarios, explicitly comparing all facilities with hospitals only. We model walking speeds appropriate for caregivers with young children under wet-surface conditions, generate population-weighted delta travel times per parish, and intersect impacts with a nutrition-sensitive vulnerability index derived from WorldPop development indicators [37]. We ask: (1) How do floods in Kampala alter travel time to healthcare facilities that deliver nutrition-sensitive MNCH services, both across all public/PNFP facilities and for hospitals only? and (2) How are these effects distributed across nutrition-sensitive vulnerability strata?

We hypothesise that short-duration, high-intensity storms will disproportionately degrade access in high-vulnerability parishes and that hospital access losses will exceed losses to all facilities, reflecting spatial scarcity. By aligning geospatial accessibility modelling with a nutrition-sensitive lens, the study produces spatially targetable evidence for implementing Uganda's Health National Adaptation Plan (2025–2030), the RMNCAH Sharpened Plan II, and Kampala's Disaster Risk & Climate Resilience Strategy [38–41]. The findings aim to support the Ministry of Health and the Kampala Capital City Authority (KCCA), by translating flood-impact modelling into actionable evidence for health system planning and climate adaptation.

Methods

We designed a geospatial analysis to quantify flood-induced changes in nutrition-sensitive geographical healthcare accessibility to public and PNFP healthcare facilities in Kampala. We focused on these facilities under the working assumption, consistent with the Lancet's nutrition-sensitive framing and UNICEF's systems approach, that they are the primary delivery platforms for routine MNCH contacts that provide counselling, supplementation, growth monitoring, and immunisation [13,14,42,43]. Accordingly, we operationalised a nutrition-sensitive lens that prioritises timely contact with delivery platforms rather than nutrition status itself. We modelled two tiers: all facilities, the nearest public or PNFP facility at any level, indexing access to routine MNCH contacts, and hospitals only, the nearest public or PNFP hospital, indexing access to referral and comprehensive care [44].

Study area

Kampala (see Figure 1), the capital and largest city of Uganda, is situated in East Africa and has been identified as one of the most vulnerable cities globally to the impacts of climate change due to its rapid urbanization, geographical features, and inadequate infrastructure [45]. It is also one of the fastest growing cities in Africa with an estimated annual population growth rate of 5.6% [46] which has led to considerable socio-economic and environmental challenges [29,47–49]. Kampala's unique topography, consisting of seven hills, valleys, and interspersed wetlands, coupled with its proximity to Lake Victoria, makes it particularly susceptible to pluvial floods; floods caused by heavy rainfall rather than river overflow [28].

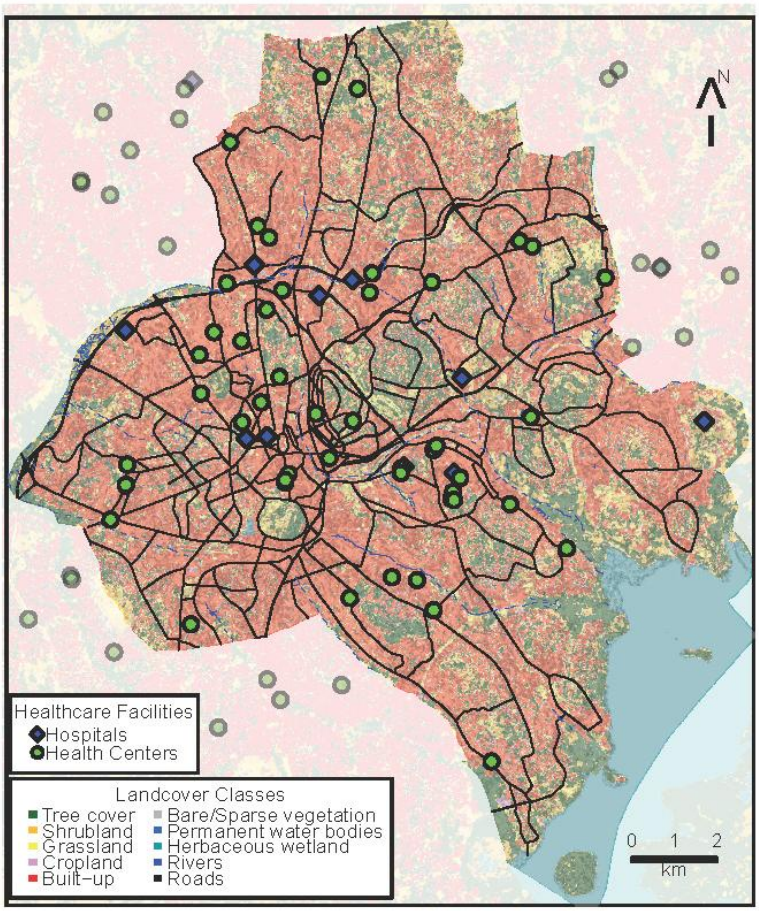

Figure 1 | Baseline geography and public healthcare infrastructure in Kampala, Uganda.
Map displays the study area's land cover, hydrography, transport network, and locations of public healthcare facilities, with a 0–2 km scale bar and a north arrow for orientation. Colors encode land cover classes as indicated in the legend, tree cover, shrubland, grassland, cropland, built up, bare or sparse vegetation, permanent water bodies, and herbaceous wetland. Linear symbology distinguishes rivers from roads. Point symbols distinguish hospitals from health centres. Abbreviations, km kilometers, N north.

The city's infrastructural inadequacies are especially evident in its drainage systems, which are often insufficient to manage the heavy rainfall [3,30].

Kampala's rainfall disruptions are frequent under its current climate, daily totals of at least 20 mm occurred on average 22 times per year during 1993–2015 [50]. Other metrics, such as the city's intensity–duration–frequency relationships map depths to return periods, for example a 2-hour rainfall event of 58.2 mm and 91.7 mm correspond to approximately 2-year and 10-year events, respectively [51]. Consistent with empirically observed sub-daily extremes, a 1-hour intensity near 75 mm has been recorded in Kampala and aligns with the 20-year return level from the historic IDF table [50]. News catalogue analysis found 41 media-reported floods occurred during 2000–2016, roughly 2.5 events per year, clustering around the ~20 mm daily threshold [50].

Geographic accessibility model

Data sources and pre-processing

Our analysis was conducted at the parish level, using Kampala's 96 parishes with their 2016 boundaries [54]. Input layers comprised a digital elevation model [55], land cover [56], the road network [57], hydrography [57,58], public and PNFP health facilities [59], population counts [60], and development indicators [37]. A complete table summarizing the data, including names and producers, appears in Supplementary Table 1. All datasets were projected to UTM Zone 36N. Open Street Map (OSM) highways were restricted to motorway, trunk, primary, secondary, tertiary, with link variants collapsed to their parent class. Water lines were restricted to rivers, streams, and canals. To ensure consistent spatial support, the 100 m WorldPop population surface was disaggregated to 10 m by block averaging, splitting each 100 m cell into a 10×10 grid and dividing values by 100, which preserves parish totals. The DEM was resampled to the 10 m grid using a bilinear scheme and land cover using nearest neighbour resampling.

AccessMod pipeline and iterative travel time layers

Accessibility modelling was performed using AccessMod 5 software [61,62], a WHO-supported GIS tool that estimates travel time to healthcare facilities based on terrain, land cover, road networks, and

transport modes. A baseline merged land-cover, MLC0, was created from land cover, roads, hydrography, and DEM, with rivers and lakes treated as barriers except at mapped road crossings. Pluvial flood polygons were provided with rainfall intensity, 20, 40, 60, 80, 100 mm, duration, 1, 3, 6 hours, and water-depth thresholds, 0.10, 0.20, 0.30 m. For each of the 15 rainfall–duration scenarios, flood polygons were rasterised to the 10 m grid and overlaid on MLC0 to build a scenario-specific merged land cover (see Supplementary Figure 1). Batch execution used an adapted replay workflow of AccessMod that loops through multiple merged land-covers to generate scenario-specific travel-time rasters (see the forked GitHub project for implementation details [63]).

Travel mode and scenario parameterization

We modelled walking as the primary mode for adults accompanying young children, consistent with travel patterns among low-income households and those without access to motorized transport [34]. Parameter choices were validated in the United Nations Population's Fund (UNFPA's) Travel Scenario Workshops [64] held in Kampala, 2–6 December 2024. Participants were local experts drawn from the Ministry of Health, UNFPA, KCCA, and Ugandan universities, spanning health informatics, geospatial analysis, and public health. They had direct operational knowledge of how caregivers and their children travel to care in Kampala, including usual modes, costs, speeds, and barriers, which informed assumptions on travel speeds, flood-related impediments, and facility functionality. The travel scenario workshop elicited expert knowledge as detailed in Molenaar et al. [65]. Participants confirmed the walking-with-children speed provided by Watmough et al. [66] and also the flood-adjusted travel speeds which were derived from Makanga et al. [67]. Makanga et al. [67] estimate a 20% speed reduction on paved and 30% reduction on unpaved surfaces during wet conditions. Baseline and flood-phase walking speeds by land cover and road class are shown in Table 1. The participants concluded that it was assumed that 10 cm of floods was traversable like wetlands and have been treated as such. Floods of 20 and 30 cm have been deemed barriers to movement, not necessarily because such depths are entirely impassable, but because workshop participants signified that local depths may exceed the data's resolution.

Outcome: population-weighted delta travel time & vulnerability stratification

Travel time, in minutes, was computed via an anisotropic least-cost path algorithm applied to the merged land-cover surfaces. The walking speeds (towards the health facilities) are corrected by the slopes derived from the DEM, according to the Tobler equation [68]. For each flood scenario we produced two travel-time rasters, one to the nearest public or PNFP facility of any level, and one to the nearest public

Table 1. Walking speed, km h^{-1}, by land cover and road class under baseline and flood phases

Landcover	Speed (km/hr.)	
	Baseline (walking)	Floods phase (walking)
Trunk road	3.9	3.120
Primary road	3.9	3.120
Motorway	3.9	3.120
Secondary road	3.51	2.808
Tertiary road	3.51	2.808
Tree cover	1.17	0.819
Shrubs	1.17	0.819
Grassland	2.34	1.638
Agriculture	2.34	1.638
Bare[1]	0.89	0.623
Urban	1.17	0.936
Herbaceous wetland	0.89	0.623
Water bodies	0	0
Floods 10 cm	NA	0.623
Floods 20 cm	NA	0
Floods 30 cm	NA	0

[1]Areas identified as 'Bare Areas' within the Sentinel-2 LULC 2016 for Uganda were primarily dry riverbed or sandbanks within rivers (Watmough et al., (2022))

or PNFP hospital, with baseline rasters using MLC0 and flood rasters using the 15 scenario-specific layers with corrections and barriers as specified above. For each parish p and scenario s, the primary outcome was the population-weighted mean change in travel time relative to baseline over populated cells that remained reachable in both conditions (see Supplementary Methods 1 for a detailed step-by-step calculation):

$$Weighted\ \Delta T_{\text{Parish}} = \frac{\sum_{i=1}^{n} \left(\Delta T_{\text{cell}_i} \times \text{Population Count}_{\text{cell}_i} \right)}{\sum_{i=1}^{n} \text{Population Count}_{\text{cell}_i}}$$

To examine vulnerability, we constructed a nutrition-sensitive vulnerability index from WorldPop developmental indicator that reflect determinants of undernutrition: mothers without

antenatal care, without postnatal care, without tetanus toxoid before birth, without health insurance, birth without a skilled attendant, underweight, vaccination status for DTP1, DTP3, and MCV1, malaria incidence, children in the poorest households, mothers without formal education, large households with at least nine members, and women's limited decision-making autonomy. To maximize interpretability we used equal weights, following Utazi et al. [37], who demonstrated that principal-component or factor-analytic weightings produce spatial patterns highly similar to those from simple averaging for WorldPop indicators. Each indicator was min–max rescaled to 0–100 and averaged to a continuous cell-level score:

$$V_i = \frac{1}{n}\sum_{k=1}^{n} I_{k,i}$$

Where:

- V_i = vulnerability score for cell i
- n = total number of indicators
- $I_{k,i}$ = normalized value (scaled 0–100) of indicator k at cell i

The V_i was classified into quartiles Q1–Q4, with Q4 denoting highest vulnerability. We overlaid quartile masks on ΔT rasters to summarise $\Delta\bar{T}_p$ by vulnerability strata and to derive bivariate maps that highlight parishes experiencing jointly high vulnerability and large losses in geographical access. Full indicator definitions appear in Supplementary Methods 2, and Supplementary Figure 2 provides the equal-weight vulnerability-index raster and a misclassification comparison with a PCA-based index which we did not use in our main analyses.

Use of large language model (LLM).

ChatGPT (GPT-5, OpenAI) was used solely to support language and structure editing. All scientific content, analysis decisions, and interpretations were developed and verified by the authors.

Data and code availability

All datasets used in this study are publicly accessible and fully documented in Supplementary Table 1. The minimum dataset required to reproduce the findings is archived on Zenodo under DOI: (URL to be added after peer-review). The complete analysis workflow is available on GitHub: (URL to be added after peer-review). All data was processed and visualized using R version 4.4.0 [69].

Results

Baseline geographical healthcare accessibility

Under baseline conditions, our analyses show spatial disparities in geographical healthcare accessibility within Kampala. Accessibility to public and PNFP healthcare facilities varies, travel times are shortest in the inner portion of the extent and are substantially longer toward the outer edges of the extent (see Figure 2). Panel (a) illustrates baseline accessibility to all public and PNFP healthcare facilities, while panel (b) focuses on public and PNFP hospitals only. In panel (a), most parishes fall within the shortest travel time ranges, reflecting the wider distribution of both hospitals and lower-level facilities. In contrast, panel (b) shows more limited and fragmented coverage of short travel times due to the smaller number of hospital locations. In panel (b), travel times increase toward the urban periphery, especially in the northern, eastern, southern and south-western regions, where values commonly exceed 120 minutes (depicted in orange and red).

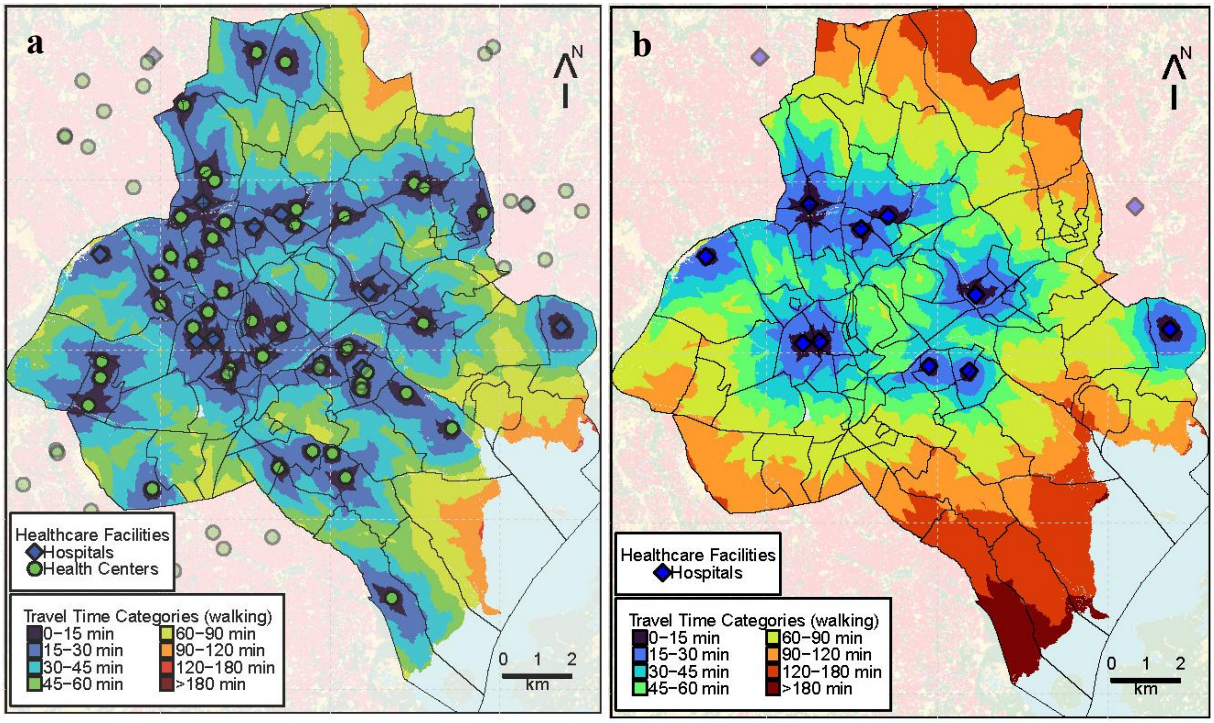

Figure 2 | Baseline walking travel time to healthcare in Kampala, Uganda.
Maps depict population surface travel time, walking only, from any location to the nearest healthcare service under baseline conditions. Travel time is classified into eight categories, 0–15, 15–30, 30–45, 45–60, 60–90, 90–120, 120–180, and >180 minutes, encoded with a sequential light to dark palette where darker shading indicates longer travel time. Point symbols mark facility locations and distinguish hospitals from health centres where applicable. A scale bar, 0–2 km, and a north arrow provide orientation. Abbreviations, min minutes, km kilometers, N north. Symbology and class breaks are identical across panels to enable visual comparison.

a, Nearest any public healthcare facility.
Travel time to the nearest facility of any type is shown using the eight class scheme above. Point symbols identify hospitals and health centres.
b, Nearest hospital only.
Travel time to the nearest hospital is mapped using the same classes and shading as in panel a. Only hospitals are shown in the facility layer for this panel.

Flood-induced changes in healthcare accessibility, all facilities versus hospitals

To evaluate flood-induced changes in healthcare accessibility, we simulated 15 distinct pluvial flood scenarios derived from a combination of five rainfall intensities (20, 40, 60, 80, 100 mm) and three durations (1, 3, 6 hours). The resulting changes are quantified using the population-weighted change in travel time at the parish level, expressed as an increase relative to baseline. Summary statistics are

provided in Table 2, spatial patterns are presented in Figure 3 & 4, and violin distributions visualized in Figure 5.

Across the 15 scenarios, travel time increased city-wide for both tiers, with systematically larger penalties for hospitals than for all facilities, see Table 2, Figures 3–5. For all facilities, means ranged from 11.2 minutes under 20 mm, 6 hours to 19.1 minutes under 100 mm, 1 hour, medians were 10–12 minutes, interquartile ranges were compact, and the maximum parish-level increase reached 193 minutes. For hospitals, means ranged from 23.0 to 55.8 minutes over the same envelope, medians were 21–42 minutes, distributions were broader, and maxima reached 275 minutes. Duration gradients were consistent at fixed intensity, for example at 60 mm the all-facilities mean stepped down from 17.3 to 14.5 to 12.9 minutes as duration increased from 1 to 3 to 6 hours, and at 40 mm the hospital mean stepped down from 44.0 to 34.6 to 31.6 minutes.

Distributions were right-skewed in both tiers, see Figure 5, with narrower, lower violins for all facilities and taller, heavier-tailed violins for hospitals, especially for short, intense events. Spatially, Figures 3–4 show the central urban core concentrated in low-delay classes for all facilities, 0–30 minutes, while peripheral belts accumulate 30–60+ minute increases for hospitals under 60–100 mm, 1 hour, with deep-purple pockets extending north-east. At 3- and 6-hour durations the same geography persists but typically steps down one bin, many peripheral parishes moving from 60+ minutes to 30–60 minutes, while the core remains predominantly low-delay.

Table 2 – Summary of Population-Weighted Changes in Travel Time to Healthcare Facilities Under Simulated Flood Scenarios in Kampala, by Rainfall Duration and Intensity

		All Facilities						Hospitals					
Duration	**Intensity**	Mean	Min	Q25	Median	Q75	Max	Mean	Min	Q25	Median	Q75	Max
1hr	20	12.8	0	6	10	16	77	28.7	0	14	25	38	156
1hr	40	15.9	0	6	11	19	117	44.0	0	16	33	61	204
1hr	60	17.3	0	6	11	22	116	47.9	0	16	37	69	206
1hr	80	18.4	0	7	12	23	120	52.3	0	18	40	74	230
1hr	100	19.1	0	7	12	24	193	55.8	0	19	42	79	241
3hr	20	12.1	0	6	10	15	115	27.3	0	13	24	38	135
3hr	40	13.2	0	6	10	16	116	34.6	0	14	25	46	182
3hr	60	14.5	0	6	11	17	164	36.9	0	15	27	49	250
3hr	80	15.3	0	6	11	18	121	40.2	0	15	29	56	251
3hr	100	15.9	0	6	11	19	117	44.6	0	16	32	64	275
6hr	20	11.2	0	6	10	14	111	23.0	0	13	21	31	99
6hr	40	12.7	0	6	10	15	142	31.6	0	13	24	41	177
6hr	60	12.9	0	6	10	16	147	33.8	0	14	25	45	181
6hr	80	13.2	0	6	10	16	153	35.5	0	14	25	50	181
6hr	100	14.0	0	6	10	17	141	37.1	0	15	27	53	183

NB: Delta travel time values represent the population-weighted change in minutes in accessibility to healthcare facilities under simulated flood scenarios, relative to baseline conditions. Intensity refers to total rainfall in millimetres, and Duration to the duration of rainfall events.

Figure 3 | Population-weighted change in walking travel time to the nearest public healthcare facility across rainfall–duration flood scenarios in Kampala, Uganda.

Each panel maps the mean population-weighted increase in travel time relative to baseline, Δ travel time in minutes, to the nearest public facility of any type under the indicated rainfall intensity and storm duration. Choropleth shading encodes three classes of Δ travel time, 0–30, 30–60, and >60 minutes, with darker shading indicating larger increases. An auxiliary legend classifies total population per spatial unit, Population Sum, into 0–10,000, 10,000–30,000, and ≥30,000. Symbology and class breaks are identical across panels to enable direct comparison. Abbreviations, mm millimetres, h hours, min minutes, Δ travel time change in travel time.

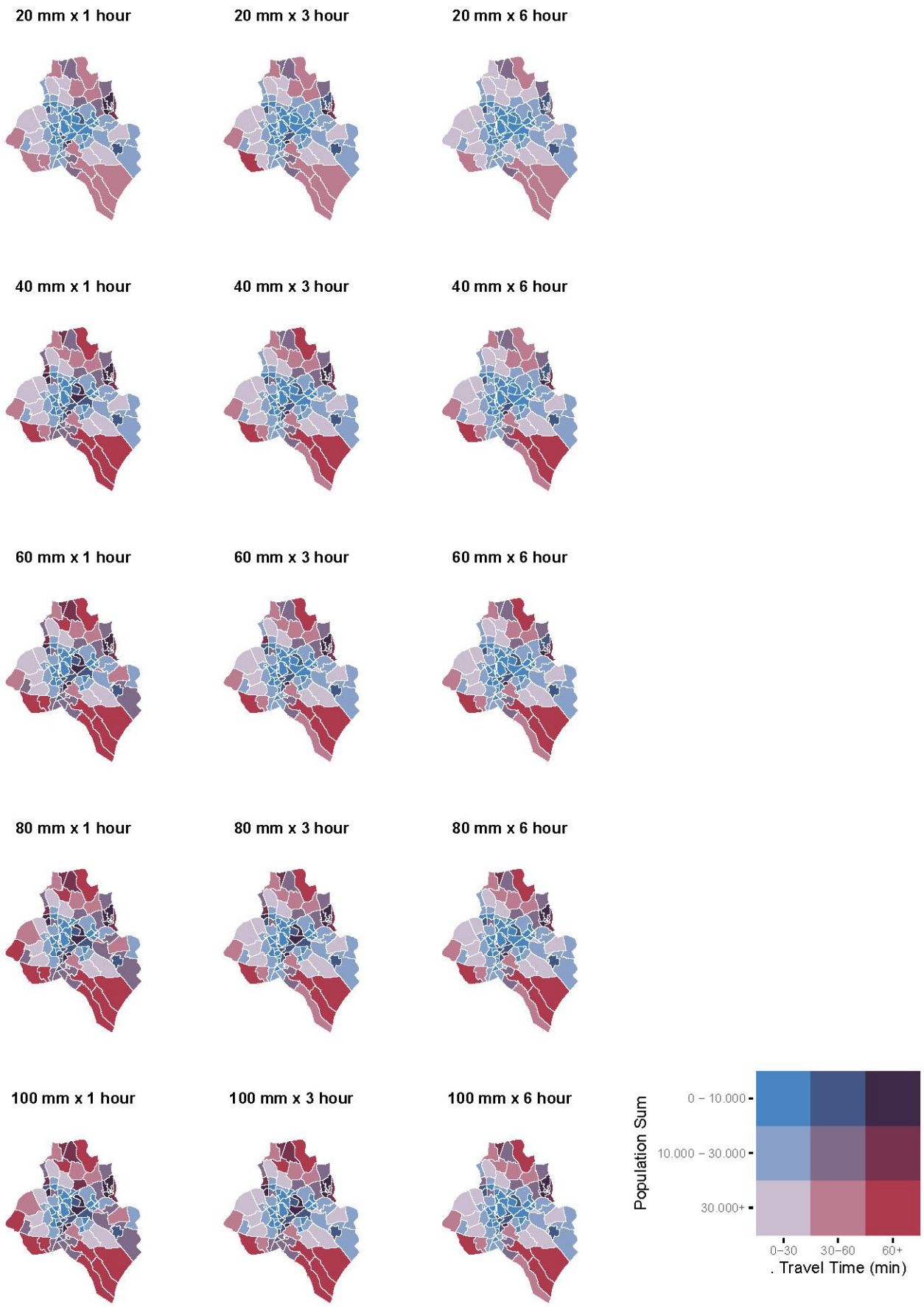

Figure 4 | Population-weighted change in walking travel time to the nearest public hospital across rainfall–duration flood scenarios in Kampala, Uganda.

Each panel maps the mean population-weighted increase in travel time relative to baseline, Δ travel time in minutes, to the nearest public hospital under the indicated rainfall intensity and storm duration. Choropleth shading encodes three Δ travel time classes, 0–30, 30–60, and >60 minutes, with progressively darker shading indicating larger increases. An auxiliary legend classifies total population per spatial unit, Population Sum, into 0–10,000, 10,000–30,000, and ≥30,000, with classes displayed consistently across panels. Symbology, map projection, and class breaks are identical in all panels to enable direct comparison. Abbreviations, mm millimetres, h hours, min minutes, Δ travel time change in travel time.

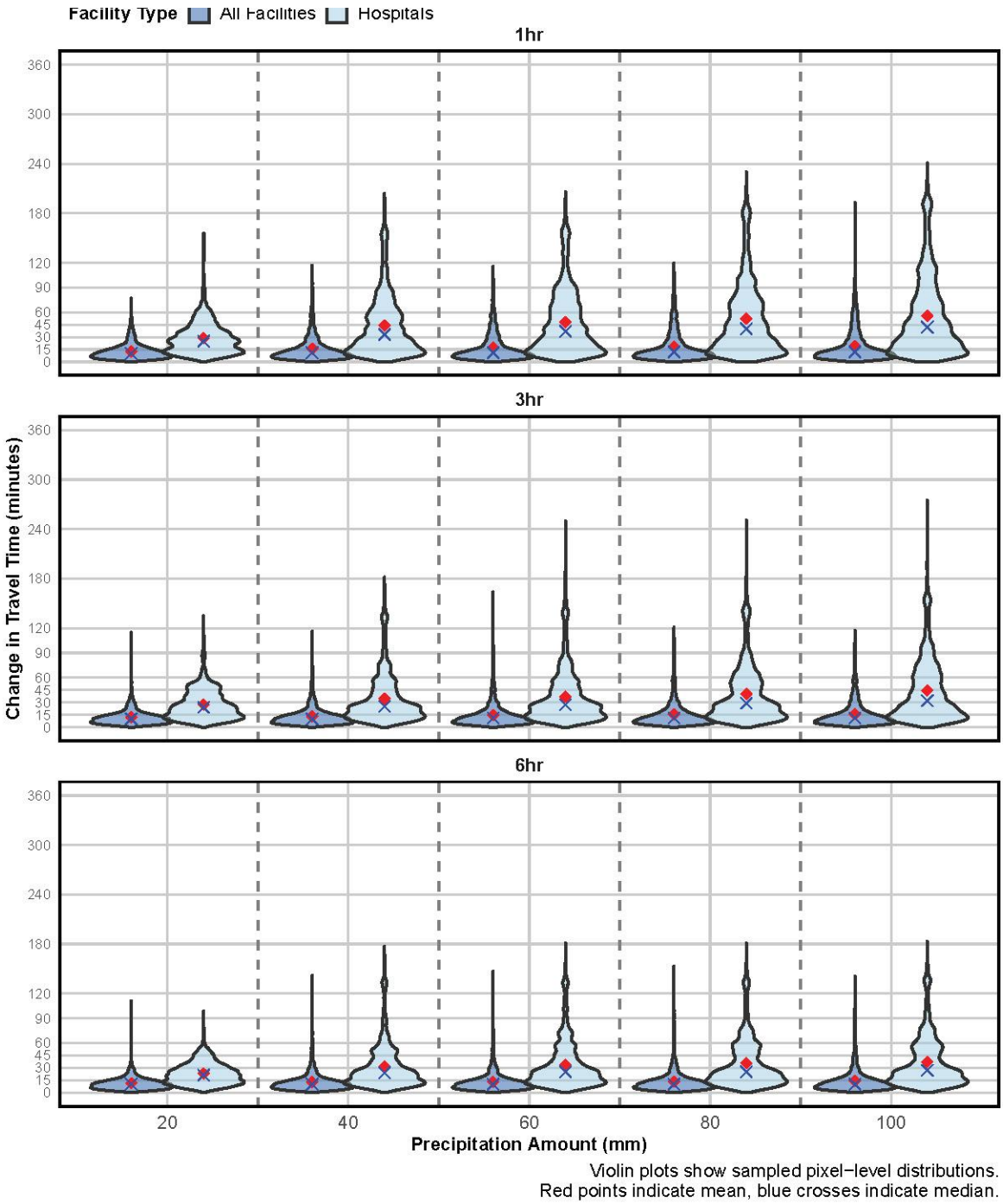

Figure 5 | Change in walking travel time across rainfall–duration scenarios for all facilities and hospitals in Kampala, Uganda.

Violin plots depict sampled pixel-level distributions of the change in travel time, minutes, from baseline to the nearest service for each rainfall intensity on the x-axis, 20, 40, 60, 80, 100 mm. Two violins are shown per intensity, one for all public facilities and one for hospitals. Violin width reflects kernel density. Red points mark the mean and blue crosses mark the median in each distribution. The y-axis shows change in travel time in minutes, 0–360 in the figure. Fill colours indicate facility type, All facilities and Hospitals, and are held constant across panels. Abbreviations, mm millimetres, min minutes, h hours.

Nutrition-sensitive access impacts across vulnerability strata

To examine how flood-related disruptions to healthcare accessibility were distributed across different vulnerability subgroups, we assessed the vulnerability composition of those experiencing increased travel time. Summary data are in Table 3, spatial patterns in Figures 6–7, and quartile violin distributions in Figure 8.

Across vulnerability quartiles (Q1–Q4), population-weighted mean increases in travel time rose with precipitation intensity and were highest for 1-hour events. For all facilities, means ranged from 9.9 minutes under 20 mm, 6 hours (Q1) to 24.2 minutes under 100 mm, 1 hour (Q3), with compact interquartile ranges and maxima of 199.9 minutes. For hospitals, delays were substantially larger and more variable, with the highest mean in Q4 under 100 mm, 1 hour (97.6 minutes, median 82.8, Q75 142.2, max 322.4). At fixed scenarios, both intensity and vulnerability gradients were evident: at 40 mm, 1 hour, hospital means rose from 38.2 minutes in Q1 to 73.8 minutes in Q4, while all-facility means stayed relatively the same, from 19.6 to 19.0 minutes across the same quartiles. The Q4–Q1 contrast at 100 mm, 1 hour reached 54.5 minutes for hospitals but only 1.7 minutes for all facilities.

In Figure 8, both tiers display right-skewed distributions, with narrower, lower violins for all facilities and broader, heavier-tailed violins for hospitals. Within each vulnerability quartile, distributions shift upward with intensity and shorten with duration. Across quartiles, Q3 and Q4 violins sit slightly higher than Q1–Q2 for all facilities, while the difference is pronounced for hospitals, particularly at 80–100 mm, 1 hour.

The bivariate maps, Figures 6–7, reveal that most parishes remain in the 0–30 minute class across scenarios, but under 80–100 mm, 1 hour, highly vulnerable (Q4) southern and south-eastern parishes experience the largest increases. For hospital access, these areas move into the highest combined categories of vulnerability and delay (>120 minutes), with additional northern periphery pockets also shifting upward. Central parishes remain largely within low-delay classes across durations, reflecting proximity to hospitals.

Table 3 – Population-Weighted Delta Travel Time to Healthcare Facilities Under Urban Flood Scenarios by Rainfall Intensity, Duration, and Vulnerability Quartile in Kampala

Duration	mm	Vulnerability	All facilities						Hospitals Only					
			Mean	Min.	Q25	Median	Q75	Max	Mean	Min.	Q25	Median	Q75	Max
1hr	20	Q1	12.1	0	5.0	8.5	14.4	114.3	22.1	0.0	9.8	16.2	28.1	149.5
1hr	20	Q2	15.3	0	6.2	10.5	18.3	119.0	32.4	0.0	18.3	29.4	41.0	202.4
1hr	20	Q3	17.0	0	9.2	15.7	22.6	75.7	39.8	0.6	20.8	33.7	53.0	213.3
1hr	20	Q4	17.3	0	9.4	15.4	22.2	95.6	43.3	0.5	25.7	41.3	57.3	128.0
1hr	40	Q1	19.6	0	5.2	9.7	18.6	199.9	38.2	0.0	10.4	19.2	49.0	258.7
1hr	40	Q2	18.8	0	6.3	11.2	22.2	159.3	45.4	0.0	19.9	33.5	58.3	264.9
1hr	40	Q3	19.3	0	9.4	16.7	25.6	112.3	56.1	0.6	23.8	43.8	79.3	246.3
1hr	40	Q4	19.0	0	9.5	16.2	23.9	114.9	73.8	0.5	34.8	66.8	100.4	260.0
1hr	60	Q1	20.8	0	5.5	10.1	20.1	197.4	40.0	0.0	10.6	20.2	52.2	282.4
1hr	60	Q2	19.8	0	6.4	11.6	23.2	151.3	48.3	0.0	20.8	35.4	62.8	289.8
1hr	60	Q3	21.3	0	9.4	17.1	28.2	130.4	63.5	0.6	25.6	53.3	89.6	258.5
1hr	60	Q4	21.3	0	9.6	16.7	26.7	126.5	80.2	0.5	40.7	71.7	114.0	263.3
1hr	80	Q1	21.3	0	5.6	10.4	20.6	191.5	41.8	0.0	10.9	21.2	53.8	295.2
1hr	80	Q2	21.5	0	6.5	12.1	24.0	151.5	52.9	0.0	22.0	38.0	68.2	309.5
1hr	80	Q3	23.3	0	9.8	17.7	29.1	135.1	69.9	0.6	27.1	57.8	97.6	296.8
1hr	80	Q4	22.5	0	9.8	17.4	28.1	133.0	89.7	0.5	43.7	77.1	128.0	304.2
1hr	100	Q1	21.8	0	5.8	10.9	21.3	190.6	43.1	0.0	11.1	22.1	55.6	320.7
1hr	100	Q2	22.1	0	6.6	12.3	24.6	188.5	55.6	0.0	22.8	40.2	70.4	326.4
1hr	100	Q3	24.2	0	10.1	18.2	30.2	138.6	75.2	0.6	27.7	60.3	105.3	321.5
1hr	100	Q4	23.5	0	10.0	18.1	30.3	136.2	97.6	0.5	46.8	82.8	142.2	322.4
3hr	20	Q1	12.0	0	4.9	8.4	13.6	140.4	21.9	0.0	9.5	15.4	27.6	181.9
3hr	20	Q2	13.8	0	6.1	10.0	16.7	151.5	33.0	0.0	17.3	28.7	41.5	189.7
3hr	20	Q3	16.5	0	8.9	15.2	21.3	109.6	36.4	0.6	19.3	31.7	48.7	161.4
3hr	20	Q4	15.5	0	9.2	14.4	20.1	80.3	40.3	0.5	24.7	39.0	54.3	109.4
3hr	40	Q1	13.1	0	5.0	8.7	15.3	140.4	25.2	0.0	10.0	17.1	31.1	196.3
3hr	40	Q2	16.4	0	6.2	10.5	18.5	149.9	38.6	0.0	18.3	30.0	46.2	210.2
3hr	40	Q3	17.5	0	9.2	15.8	22.5	106.8	45.2	0.6	20.7	34.4	62.5	217.5
3hr	40	Q4	16.1	0	9.3	14.7	20.6	80.3	55.9	0.5	26.5	46.7	73.6	224.0
3hr	60	Q1	17.4	0	5.0	9.0	16.0	196.5	30.5	0.0	10.1	17.5	37.1	203.5
3hr	60	Q2	17.0	0	6.2	10.7	19.6	151.3	39.9	0.0	18.6	30.8	48.0	218.8
3hr	60	Q3	18.2	0	9.3	16.1	23.8	109.6	48.8	0.6	21.5	36.8	67.0	263.0
3hr	60	Q4	17.9	0	9.4	15.5	22.7	95.6	59.3	0.5	27.8	49.7	77.3	273.5
3hr	80	Q1	18.6	0	5.1	9.3	17.6	195.7	35.8	0.0	10.3	18.5	41.3	260.4
3hr	80	Q2	17.5	0	6.2	10.9	20.8	155.5	41.5	0.0	19.0	31.7	50.9	244.7

Table 3 – Population-Weighted Delta Travel Time to Healthcare Facilities Under Urban Flood Scenarios by Rainfall Intensity, Duration, and Vulnerability Quartile in Kampala

Duration	mm	Vulnerability	All facilities						Hospitals Only					
			Mean	Min.	Q25	Median	Q75	Max	Mean	Min.	Q25	Median	Q75	Max
3hr	80	Q3	18.7	0	9.3	16.4	24.6	148.9	52.2	0.6	22.4	40.1	73.2	263.0
3hr	80	Q4	18.5	0	9.4	15.6	23.1	105.3	63.0	0.5	31.0	54.3	83.7	274.5
3hr	100	Q1	19.4	0	5.3	9.7	18.5	192.3	37.4	0.0	10.4	19.0	48.2	260.4
3hr	100	Q2	19.0	0	6.2	11.1	22.1	158.1	45.8	0.0	19.4	33.5	58.5	264.9
3hr	100	Q3	19.5	0	9.4	16.7	25.8	148.9	61.0	0.6	23.4	45.8	87.2	296.3
3hr	100	Q4	18.9	0	9.5	15.8	23.5	105.3	72.6	0.5	35.0	65.2	97.6	308.5
6hr	20	Q1	9.9	0	4.8	8.1	12.8	138.8	17.5	0.0	9.2	14.4	22.8	121.3
6hr	20	Q2	12.8	0	6.0	9.7	15.5	149.9	28.4	0.0	16.5	26.4	36.2	131.6
6hr	20	Q3	15.9	0	8.7	14.8	20.5	108.2	29.3	0.6	18.4	27.9	38.9	106.3
6hr	20	Q4	15.3	0	9.0	14.0	19.9	72.0	36.0	0.5	23.2	34.2	48.0	89.8
6hr	40	Q1	12.0	0	4.9	8.4	13.9	140.4	21.9	0.0	9.6	15.5	27.4	181.9
6hr	40	Q2	15.9	0	6.0	10.0	17.7	151.5	35.3	0.0	17.4	28.8	43.2	207.3
6hr	40	Q3	16.9	0	9.0	15.4	21.8	106.8	41.0	0.6	19.4	32.2	53.7	208.8
6hr	40	Q4	15.6	0	9.3	14.4	20.1	80.3	53.0	0.5	25.2	43.6	67.6	222.4
6hr	60	Q1	12.6	0	5.0	8.6	14.7	140.4	24.5	0.0	9.9	16.4	29.8	188.3
6hr	60	Q2	16.3	0	6.2	10.5	18.3	149.9	37.8	0.0	18.1	29.9	45.4	208.7
6hr	60	Q3	17.2	0	9.2	15.7	22.2	109.6	43.3	0.6	20.1	33.7	56.5	211.7
6hr	60	Q4	15.9	0	9.3	14.6	20.4	72.0	54.9	0.5	25.9	46.2	71.4	224.0
6hr	80	Q1	13.3	0	5.0	8.7	15.3	140.4	25.2	0.0	10.0	17.2	31.5	194.7
6hr	80	Q2	16.4	0	6.2	10.6	18.5	149.9	38.8	0.0	18.2	30.1	47.0	208.7
6hr	80	Q3	17.6	0	9.2	15.8	22.7	109.6	48.0	0.6	21.0	36.5	69.0	217.5
6hr	80	Q4	16.1	0	9.3	14.7	20.6	72.0	57.3	0.5	27.7	48.8	75.3	224.0
6hr	100	Q1	16.7	0	5.1	8.9	15.5	190.6	29.7	0.0	10.1	17.4	35.9	197.9
6hr	100	Q2	16.6	0	6.2	10.6	18.8	156.8	39.4	0.0	18.3	30.4	47.7	213.1
6hr	100	Q3	17.7	0	9.3	15.9	22.9	150.2	49.3	0.6	21.2	38.1	72.1	217.5
6hr	100	Q4	16.9	0	9.4	15.2	21.6	95.6	58.9	0.5	28.6	50.6	77.3	228.9

NB: Disaggregated statistics by vulnerability quartile exclude raster cells with missing values in the vulnerability index, which may occur due to differences in spatial resolution and alignment between input layers. As a result, extreme values (such as the maximum delta travel time) may be slightly lower in the disaggregated summaries compared to the overall population-weighted estimates.

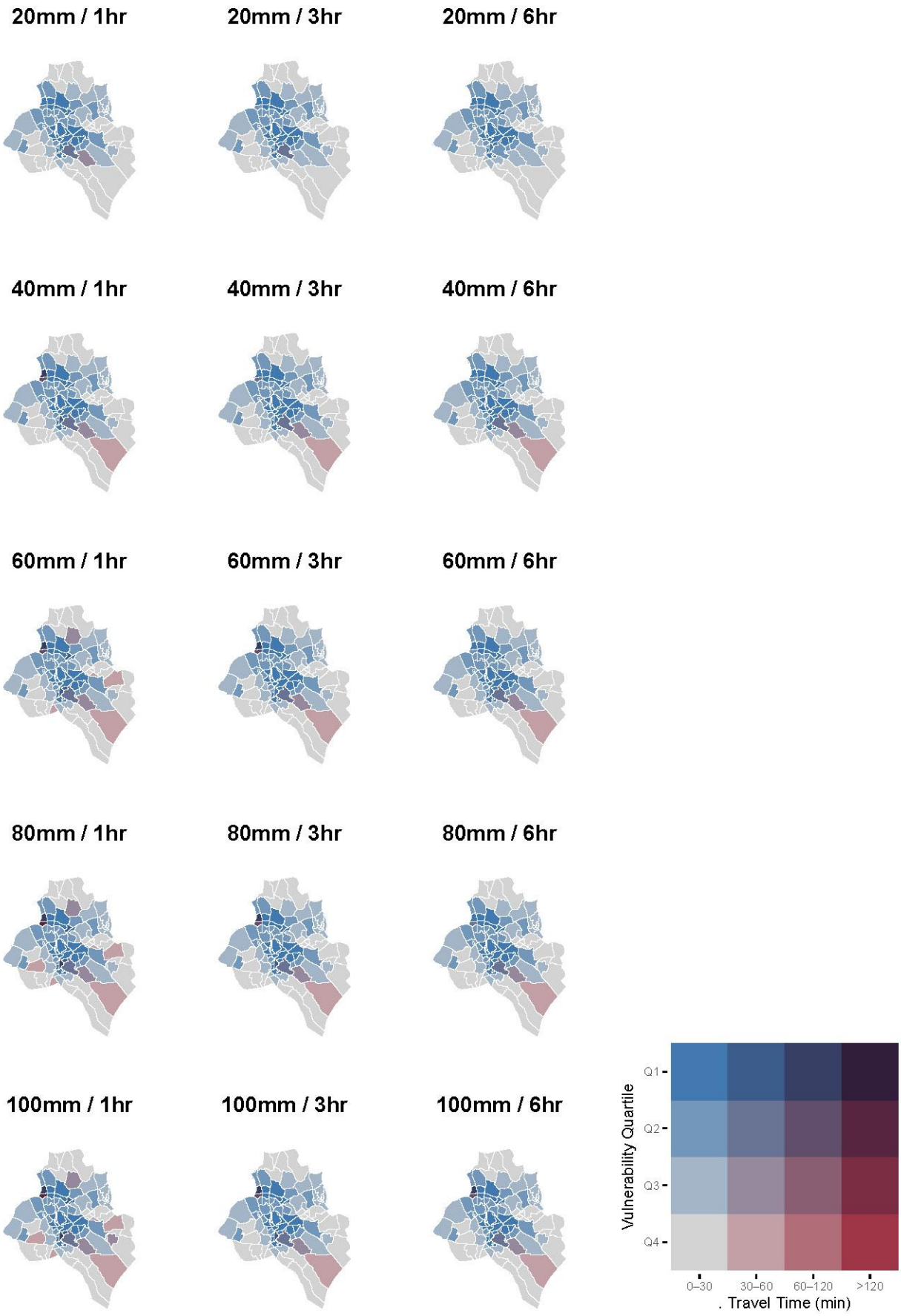

Figure 6 | Population-weighted mean change in walking travel time to the nearest public healthcare facility by vulnerability quartile across rainfall–duration flood scenarios in Kampala, Uganda.
Each panel summarizes the population-weighted mean Δ travel time, minutes, relative to baseline for four vulnerability quartiles, Q1 low to Q4 high, under the specified rainfall intensity and storm duration. Within each panel, the y-axis lists vulnerability quartiles and the colour of each bar or tile encodes the corresponding Δ travel time class, 0–30, 30–60, 60–120, and >120 minutes, with progressively darker shading indicating larger increases. Symbology and class breaks are identical in all panels to enable direct comparison. Abbreviations, mm millimetres, h hours, min minutes, Δ travel time change in travel time.

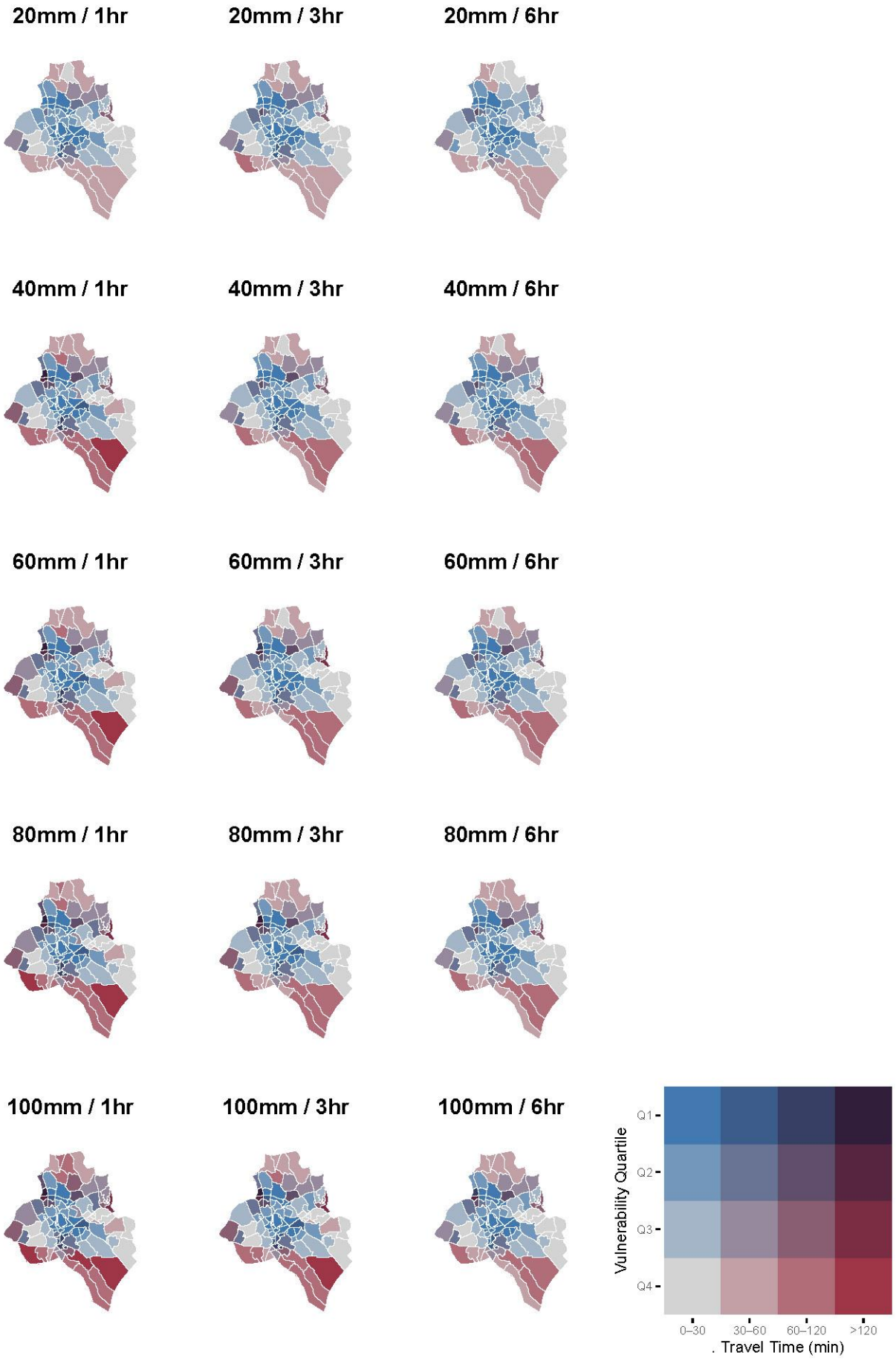

Figure 7 | Population-weighted mean change in walking travel time to the nearest public hospital by vulnerability quartile across rainfall–duration flood scenarios in Kampala, Uganda.
Each panel summarizes the population-weighted mean Δ travel time, minutes, relative to baseline for four vulnerability quartiles, Q1 low to Q4 high, under the specified rainfall intensity and storm duration. Within each panel, the y-axis lists vulnerability quartiles and the fill colour encodes Δ travel time classes, 0–30, 30–60, 60–120, and >120 minutes, with progressively darker shading indicating larger increases. Class limits, colour mapping, axes, and projection are identical across panels to enable direct comparison. Abbreviations, mm millimetres, h hours, min minutes, Δ travel time change in travel time.

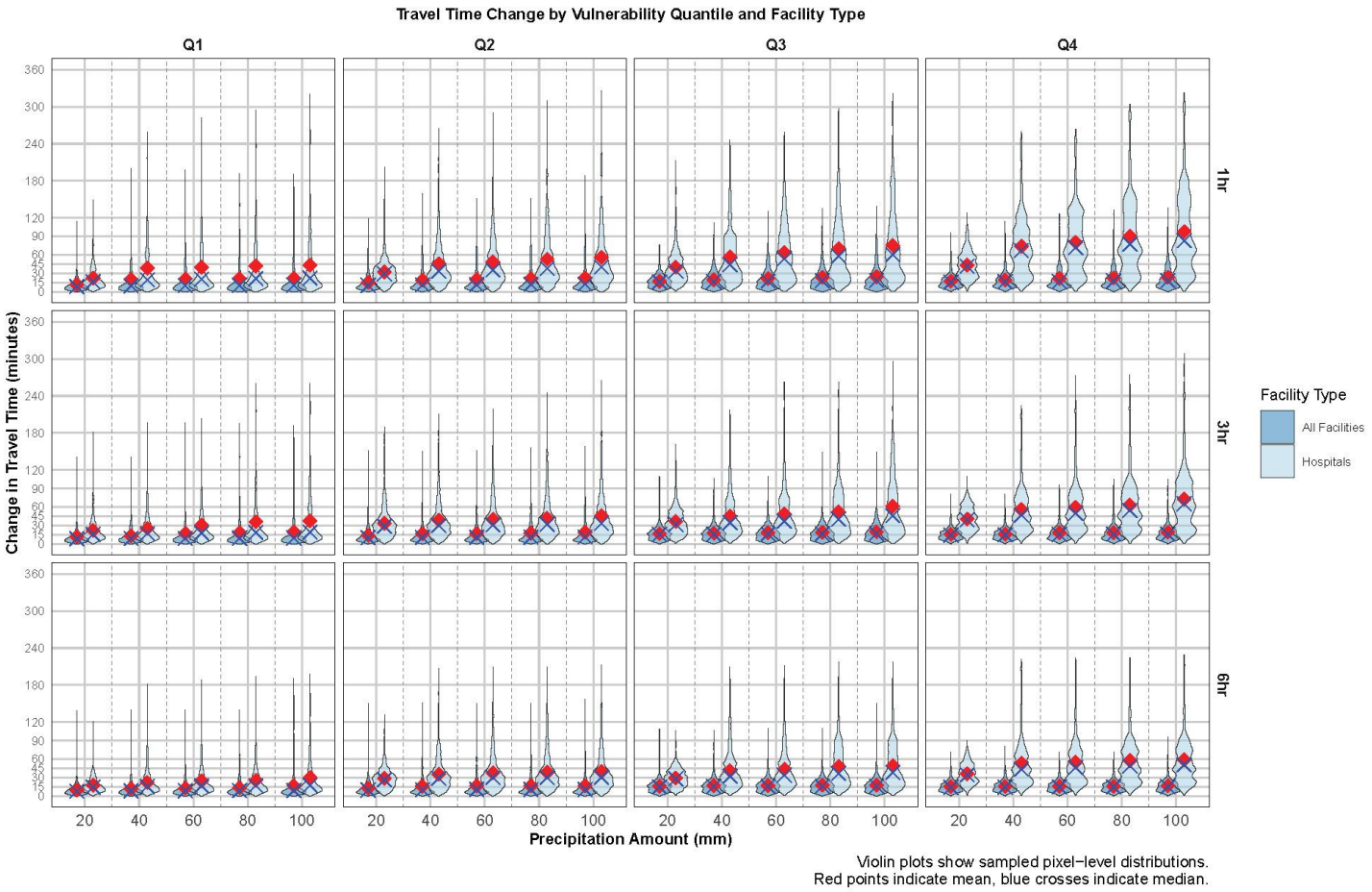

Figure 8 | Distributions of walking travel-time change by rainfall intensity, storm duration, vulnerability quartile, and facility type in Kampala, Uganda.
Violin plots show sampled pixel-level distributions of the change in travel time from baseline, Δ minutes on the y-axis, to the nearest service as rainfall intensity increases on the x-axis, 20, 40, 60, 80, 100 mm. For each intensity, two violins are plotted, one for all public facilities and one for hospitals, violin width reflects kernel density. Red points mark the mean, blue crosses mark the median, axes and symbology are identical across panels. Abbreviations, mm millimetres, h hours, min minutes, Δ change, Q1–Q4 vulnerability quartiles from low to high. Fill colours encode facility type, All facilities and Hospitals, and are held constant across panels.

Discussion

To our knowledge, we share the first high-resolution, vulnerability-disaggregated estimates of flood-induced losses in travel time to public and PNFP care healthcare facilities in Kampala. We introduce a reproducible population-weighted delta travel time metric at parish level and a tier-specific analysis that reveals structurally larger penalties for hospital access than for all facilities. By explicitly linking these delays to nutrition-sensitive indicators for mothers and children, we demonstrate that losses concentrate in the most vulnerable parishes. In the most impacted areas, population-weighted travel time to all public

and PNFP healthcare facilities increased by up to 199.9 minutes, while access to hospitals deteriorated more sharply, maxima exceeded 326 minutes, and vulnerability-quartile means approached 100 minutes under the most intense 1-hour events, while the all scenario means remained ≤24 minutes.

These accessibility losses matter for nutrition because they reduce timely contact with MNCH delivery platforms where supplementation, growth monitoring, immunisation, and caregiver counselling occur, thereby tightening the infection–undernutrition cycle in high-vulnerability parishes. Modest citywide increases to all facilities will erode timeliness and continuity of routine MNCH contacts, later ANC and PNC, delayed immunisations, fewer touchpoints for growth monitoring and IYCF counselling, with cumulative backlog effects after clustered short, intense events. By contrast, the much larger and more volatile hospital delays shift the whole distribution of time to definitive care upward, increasing referral abandonment, narrowing treatment windows for intrapartum complications and neonatal sepsis, and possibly pushing households toward informal or costly private care, heightening risk of catastrophic expenditure. The net effect is regressive, caregivers in high-vulnerability parishes who rely on walking bear disproportionate penalties, so relative inequality in timely MNCH and referral care widens even when citywide means appear moderate.

Our findings are consistent with city-scale simulations by Rentschler et al. [32], who estimated that mean travel time to hospitals in Kampala rises from 17 to 30 minutes under a 50-year flood. However, our analyses show greater increases in travel time. Even moderate increases in travel time can have severe consequences in urban poor settings, where mobility is constrained by unsafe walking environments, high transport costs, and inflexible work schedules [33]. Together, they underscore a double burden: marginalized populations are not only more exposed to floods but also experience the steepest losses in access to healthcare services. This aligns with climate–health evidence showing that those most exposed are typically least able to adapt, with vulnerability concentrated where capacities and health systems are weakest [70].

Crucially, access is not solely determined by spatial distance, as gendered and caregiving roles shape mobility. Concurrent caregiving and economic responsibilities often lead to delays or complete avoidance of formal care [71]. If travel times increase, the opportunity costs of seeking care may become

prohibitive, particularly for women managing multiple roles, resulting in postponed treatment or reliance on informal providers even in cases of acute need [33,71]. However, as evidence from Bangladesh shows, lower maternal healthcare utilisation in flood-prone areas often reflects pre-existing disadvantages, such as poverty, marginalization, and weak infrastructure, rather than the floods itself [72]. Similar findings from East and West Africa indicate that poor, remote communities face compounded barriers to hospital-based childbirth, with both poverty and distance independently driving exclusion [73]. In the absence of timely formal care, caregivers turn to informal providers or home remedies, a pattern documented in other flood-prone cities like Lagos, Nigeria [25]. Such responses, while adaptive, reflect deeper systemic failures in health system resilience and continuity. Consistent with this multidimensionality, a recent Uganda-wide analysis found no robust association between travel time to public facilities and stunting, wasting, or underweight after adjustment, hypothesizing that proximity alone is insufficient when quality, affordability, and social constraints are present [74]. These barriers are compounded by food insecurity and undernutrition, both of which are exacerbated by flood-related market and service interruptions [7,8,18,75].

Similar geographical healthcare losses due to floods have been documented elsewhere. In LMICs, Jakarta experienced 5–10 minute increases in hospital travel time during the 2013 flood [23], while post-Cyclone Idai floods in Beira saw delays exceeding 50 minutes [76]. Another study on Cyclone Idai and Kenneth in Mozambique found that travel time to the nearest functional health facility in some communities increased from 1.3 to over 63 hours [77]. Regional simulations in Southeast Asia showed average travel time increases of 38% (from 14 to 19 min.). In HICs, disruptions were more moderate: San Francisco saw a 1% drop in hospital coverage within 30 minutes [78], York (UK) experienced up to 20% loss in ambulance coverage (10-min ambulance threshold) [79], and flood scenarios in Shanghai identified that 47% of all districts were unable to be reached within a 30-min threshold [80]. However, compared to these contexts, the impact in Kampala was markedly higher. The extensive encroachment on wetlands has critically undermined the city's natural flood attenuation capacity, while unregulated expansion of informal settlements into high-risk zones has heightened exposure among already vulnerable populations [30]. Although a Drainage Master Plan was introduced to address these risks, its

implementation has been constrained by declining fiscal commitments, with budgetary allocation for flood management falling from 16.6% to 0.3% within a four-year period [31]. It should be noted that our estimates are based on a walking-only travel scenario, which are a dominant mode of transport in Kampala, whereas most comparator studies modelled motorised transport [32,77,81]. This methodological distinction likely contributes to the higher delta travel times observed in our analysis.

Looking forward, Kampala's flood impacts are likely to intensify. Projections for Lake Victoria, which shapes Kampala's rainfall, show more rain overall by mid and late century and, crucially, heavier downpours on wet days. For example, mean rain per wet day rises by about 6 percent by mid-century and 16 percent by late century, five-day totals rise by roughly 18 and 29 percent, and the heavy-rainfall tail (90^{th} – 99^{th} % precipitation events respectively (28.14; 41.17 mm/day)) widens by about 47 and 22 percent [82]. The record 2019–2020 rise in Lake Victoria levels has already been linked to human-driven climate change, which made the event about 1.8 times more likely and would have produced about 7 cm less lake-level rise in a pre-industrial climate, with floods documented along shorelines of Kampala [83]. National assessments for Uganda likewise anticipate more consecutive wet days and more days with precipitation greater than 20 mm in both rainy seasons, and report that floods have become more frequent largely due to more intense rainfall [84]. These projections indicate the need for timely actions to mitigate the impacts of urban floods.

Interpreted through a nutrition-sensitive lens, our results indicate that flood-related travel time penalties selectively erode the routine contacts through which nutrition-relevant services are provided. In the parishes with the greatest delays, missed or postponed contacts plausibly increase the risk of growth faltering and infection by limiting supplementation, vaccination timeliness, and caregiver counselling. Thus, protecting geographical access during flood shocks is a necessary, though not sufficient, condition for safeguarding child nutrition.

Policy implications

Our outputs, parish-level accessibility and vulnerability maps, can be directly used by the Ministry of Health, KCCA to prioritise infrastructure upgrades and service delivery in flood-prone areas. Our

spatially disaggregated results directly support these strategies by identifying the parishes with the highest travel time delays under 15 flood scenarios, and by overlaying these disruptions with vulnerability data. This enables policymakers to target infrastructure and service investments where inequities are most acute. These insights not only advance evidence-based planning but also support the operationalization of equitable climate adaptation.

While strategies such as the *Health National Adaptation Plan (HNAP)* (2024–2030), the *Reproductive, Maternal, Newborn, Child, Adolescent and Healthy Aging plan* (2022–2028), and the *Kampala Disaster Risk and Climate Resilience Strategy* all emphasize resilience of the health system and continuity and equity of service delivery, implementation remains inconsistent [38,40,41]. The city strategy calls for resilience standards for roads and health infrastructure, including flood-proof design, sustainable drainage and urges integration of healthcare expansion with disaster resilience planning [38]. To reduce crowding at overstretched public facilities during floods, the Ministry of Health and KCCA are advised to subsidize maternal and child services at private health facilities, a recommendation echoed in both the RMNCH Plan and KCCA planning documents [39,40]. Upgrades to flood-resilient pedestrian infrastructure should be prioritized in high-vulnerability parishes [8], particularly to improve healthcare proximity for women, which remains a key determinant of care-seeking [38].

Strengths and Limitations

This study presents several methodological strengths. First, raster-based travel time modelling offers high spatial resolution and does not rely on complete road network data, making it well-suited for heterogeneous urban areas. As Soman et al. [85] note, traditional network-based approaches often fail to represent infrastructural inaccessibility within informal settlements, where internal roads may be unmapped or inaccessible. Second, travel speeds and transport mode assumptions were validated through participatory Travel Scenario Workshops (TSWs), enhancing local relevance and accuracy. Third, the study simulates a wide range of realistic flood scenarios (n=15) that reflect Kampala's flood typologies, capturing both high-intensity short-duration and lower-intensity longer-duration rainfall events. Fourth, maternal- and child-specific considerations were integrated by applying adjusted

walking speeds based on empirical evidence, adding demographic nuance to the accessibility estimates. Finally, the alignment of travel time outputs with population-weighted vulnerability indices allows for an intersectional analysis of who is most affected and where disruptions are most severe.

However, some limitations warrant consideration. The modelling uses static, post-flood travel-time surfaces, it does not capture dynamic flood onset, peak, and recession or intra-event variability, which are characteristic of urban flood behaviour and influence access trajectories over hours to days, limiting inference on cascading effects or adaptive responses over time [86] (for implementation challenges in real-time urban flood modelling, see Piadeh et al. [87]; Kumar et al. [88]). Moreover, in dense urban settings, raster based travel time models do not reflect traffic congestion, signal timing, or routing behaviour, so they can under- or over-estimate travel times relative to traffic-aware estimates. Recent comparisons show meaningful divergences between modelled travel times and observed or API-derived times in African cities, especially during peak periods, suggesting that variability and potential underestimation should be acknowledged [81,89–91]. Although we compute at high spatial resolution, results are summarised at parish level for reporting, which may mask fine-scale disparities in exposure and access within parishes. We acknowledge a border effect. Because flood layers were available only inside the KCCA boundaries, we did not model allocations to out-of-AOI hospitals. Peripheral estimates, most visible in the north for the hospital-only scenario in Figure 2, may therefore be inflated, so inference is limited to the AOI. Extending flood layers and facility inventories beyond the boundary is a clear next step. Moreover, private-for-profit facilities, which constitute 90% of Kampala's healthcare system, were excluded due to data limitations; while public and PNFP facilities are often preferred maternal and child healthcare, this omission may understate available service options or alter accessibility patterns [39]. Finally, we did not analyse healthcare utilisation during flood periods, so the linkage from modelled accessibility to service uptake and health outcomes remains inferential rather than observed.

Conclusion

Urban floods in Kampala substantially reduces walking access to public and PNFP healthcare facilities, with disproportionally larger penalties for hospitals than for all facilities, especially during short, high-

intensity rainfall events. By modelling caregiver-appropriate speeds and a nutrition-sensitive vulnerability index, this study shows that the most vulnerable parishes experience the greatest increase in travel time, reinforcing a double burden of exposure and vulnerability. While further research is needed to link these accessibility losses to health outcomes, our findings underscore the importance of incorporating vulnerability and access metrics into urban and health system planning, to mitigate the uneven impacts of future flood events.

Acknowledgements

We gratefully acknowledge the contributions of all participants in the Travel Scenario Workshops held in Kampala, whose local expertise was essential in confirming realistic travel speeds and transport modes. We thank the representatives for their guidance, logistical support, and valuable feedback throughout the design and implementation of the accessibility modelling. Their insights greatly enhanced the contextual accuracy and relevance of this study.

Ethical approval

The Medical Ethics Review Board of the University Medical Center Groningen (METc UMCG) has classified this research as not within the scope of the Medical Research Involving Human Subjects Act. Hence, ethical approval and participant consent were unnecessary for this study.

Funding sources

We would like to acknowledge the financial support provided by the Graduate School of Medical Sciences (GSMS) from the University Medical Center Groningen (UMCG) in the form of a PhD scholarship. The GSMS/UMCG played no direct role in the study design, data collection, analysis, interpretation of data, writing of the article, or the decision to submit it for publication. The views and opinions expressed in this article are solely those of the authors and do not necessarily represent the views of the GSMS/UMCG.

Competing interests

All authors hereby state that there are no competing interests to declare. None of the project team members, collaborators, or affiliated organizations have financial, personal, or professional interests that could in any way influence or bias the research, analysis, or outcomes of this project.

Author statement

RUL: Conceptualization, Methodology, Software, Validation, Formal analysis, Data Curation, Visualization, Writing - Original Draft, Writing - Review & Editing, Project administration; GW: Conceptualization, Methodology, Resources, Supervision, Writing - Review & Editing; FH: Methodology, Software, Validation, Resources, Writing - Review & Editing; NR: Methodology, Software, Supervision, Resources, Writing - Review & Editing; FO: Investigation, Data Curation, Validation, Writing - Review & Editing; OB: Investigation, Data Curation, Validation, Writing - Review & Editing; RB: Conceptualization, Supervision, Project administration, Funding acquisition, Writing - Review & Editing.

References

1. Hirabayashi, Y., Tanoue, M., Sasaki, O., Zhou, X. & Yamazaki, D. Global exposure to flooding from the new CMIP6 climate model projections. *Sci Rep* **11**, 3740 (2021).
2. Our World in Data. Global reported natural disasters by type. *Our World in Data* https://ourworldindata.org/grapher/natural-disasters-by-type (2023).
3. Lwasa, S. Adapting urban areas in Africa to climate change: the case of Kampala. *Current Opinion in Environmental Sustainability* **2**, 166–171 (2010).
4. Lee, A. C. K., Booth, A., Challen, K., Gardois, P. & Goodacre, S. Disaster management in low- and middle-income countries: scoping review of the evidence base. *Emerg Med J* **31**, e78–e83 (2014).

5. Chen, S. *et al.* Updating global urbanization projections under the Shared Socioeconomic Pathways. *Sci Data* **9**, 137 (2022).
6. Ho Oh, E., Deshmukh, A. & Hastak, M. Disaster impact analysis based on inter-relationship of critical infrastructure and associated industries: A winter flood disaster event. *International Journal of Disaster Resilience in the Built Environment* **1**, 25–49 (2010).
7. Al-Marwani, S. Climate change impact on the healthcare provided to patients. *Bull Natl Res Cent* **47**, 51 (2023).
8. Guihenneuc, J., Ayraud-Thevenot, S., Roschnik, S., Dupuis, A. & Migeot, V. Climate change and health care facilities: A risk analysis framework through a mapping review. *Environmental Research* **216**, 114709 (2023).
9. Ebi, K. L. *et al.* Extreme Weather and Climate Change: Population Health and Health System Implications. *Annu. Rev. Public Health* **42**, 293–315 (2021).
10. Salm, L., Nisbett, N., Cramer, L., Gillespie, S. & Thornton, P. How climate change interacts with inequity to affect nutrition. *WIREs Climate Change* **12**, e696 (2021).
11. Sparling, T. M. *et al.* Intersections of Climate Change with Food Systems, Nutrition, and Health: An Overview and Evidence Map. *Advances in Nutrition* 100274 (2024) doi:10.1016/j.advnut.2024.100274.
12. UNICEF. *UNICEF Conceptual Framework on Maternal and Child Nutrition*. https://www.unicef.org/media/113291/file/UNICEF%20Conceptual%20Framework.pdf (2021).
13. Tirado, M. C. *et al.* Climate Change and Nutrition: Creating a Climate for Nutrition Security. *Food Nutr Bull* **34**, 533–547 (2013).
14. WHO. Technical series on Adapting to Climate Sensitive Health Impacts Undernutrition. https://doi.org/10.1163/9789004322714_cclc_2019-0172-659 (2019).
15. King, S. E., Sawadogo-Lewis, T., Black, R. E. & Roberton, T. Making the health system work for the delivery of nutrition interventions. *Matern Child Nutr* **17**, e13056 (2020).
16. Keats, E. C. *et al.* Effective interventions to address maternal and child malnutrition: an update of the evidence. *The Lancet Child & Adolescent Health* **5**, 367–384 (2021).

17. Bourke, C. D., Berkley, J. A. & Prendergast, A. J. Immune Dysfunction as a Cause and Consequence of Malnutrition. *Trends in Immunology* **37**, 386–398 (2016).
18. Agabiirwe, C. N., Dambach, P., Methula, T. C. & Phalkey, R. K. Impact of floods on undernutrition among children under five years of age in low- and middle-income countries: a systematic review. *Environ Health* **21**, 98 (2022).
19. Lieber, M., Chin-Hong, P., Kelly, K., Dandu, M. & Weiser, S. D. A systematic review and meta-analysis assessing the impact of droughts, flooding, and climate variability on malnutrition. *Global Public Health* **17**, 68–82 (2022).
20. Aoun, N., Matsuda, H. & Sekiyama, M. Geographical accessibility to healthcare and malnutrition in Rwanda. *Soc Sci Med* **130**, 135–145 (2015).
21. Gabrysch, S., Cousens, S., Cox, J. & Campbell, O. M. R. The influence of distance and level of care on delivery place in rural Zambia: a study of linked national data in a geographic information system. *PLoS Med* **8**, e1000394 (2011).
22. Feikin, D. R. *et al.* The impact of distance of residence from a peripheral health facility on pediatric health utilisation in rural western Kenya. *Trop Med Int Health* **14**, 54–61 (2009).
23. Klipper, I. G., Zipf, A. & Lautenbach, S. Flood Impact Assessment on Road Network and Healthcare Access at the example of Jakarta, Indonesia. **2**, 1–11 (2021).
24. Andreasen, M. H., Agergaard, J., Møller-Jensen, L., Oteng-Ababio, M. & Yiran, G. A. B. Mobility Disruptions in Accra: Recurrent Flooding, Fragile Infrastructure and Climate Change. *Sustainability* **14**, 13790 (2022).
25. Adelekan, I. O. Vulnerability of poor urban coastal communities to flooding in Lagos, Nigeria. *Environment and Urbanization* **22**, 433–450 (2010).
26. Amoako, C. & Inkoom, D. K. B. The production of flood vulnerability in Accra, Ghana: Re-thinking flooding and informal urbanisation. *Urban Studies* **55**, 2903–2922 (2018).
27. Isunju, J. B., Orach, C. G. & Kemp, J. Hazards and vulnerabilities among informal wetland communities in Kampala, Uganda. *Environment and Urbanization* **28**, 275–293 (2016).

28. Kampala Capital City Authority. *STATISTICAL ABSTRACT FOR KAMPALA CITY*. https://kcca.go.ug/media/docs/Statistical-Abstract-2019.pdf (2019).
29. Twinomuhangi, R. *et al.* Perceptions and vulnerability to climate change among the urban poor in Kampala City, Uganda. *Reg Environ Change* **21**, 39 (2021).
30. Arinabo, D. Unveiling the role of contextual factors in the evolution of urban floods in Sub-Saharan Africa: Lessons from Kampala city. *Environmental Science & Policy* **137**, 239–248 (2022).
31. Arinabo, D. Reconciling multiple forms of flood risk knowledge and institutional responses: Insights from Kampala's flood management regime. *International Journal of Disaster Risk Reduction* **94**, 103829 (2023).
32. Rentschler, J., Braese, J., Jones, N. & Avner, P. Three feet under: The impact of floods on urban jobs, connectivity, and infrastructure. (2019).
33. Janusz, K., Kesteloot, C., Vermeiren, K. & Van Rompaey, A. Daily Mobility, Livelihoods and Transport Policies in Kampala, Uganda: A Hägerstrandian Analysis. *Tijd voor Econ & Soc Geog* **110**, 412–427 (2019).
34. Foley, L. *et al.* Socioeconomic and gendered inequities in travel behaviour in Africa: Mixed-method systematic review and meta-ethnography. *Social Science & Medicine* **292**, 114545 (2022).
35. Sule, F. A. *et al.* Examining vulnerability and resilience in maternal, newborn and child health through a gender lens in low-income and middle-income countries: a scoping review. *BMJ Glob Health* **7**, e007426 (2022).
36. Pappas, A., Kovats, S. & Ranganathan, M. Extreme weather events and maternal health in low-income and middle-income countries: a scoping review. *BMJ Open* **14**, e079361 (2024).
37. Utazi, C. E. *et al.* A zero-dose vulnerability index for equity assessment and spatial prioritization in low- and middle-income countries. *Spatial Statistics* **57**, 100772 (2023).
38. World Bank & GFDRR. *Kampala Disaster Risk and Climate Change Resilience Strategy*. https://documents1.worldbank.org/curated/en/099335105132230574/pdf/P154339098e7840b309a500c9b29a6200d1.pdf (2022).

39. Kampala Capital City Authority. *A Profile of Women Seeking Maternal, Newborn, and Child Health Services in Public Facilities in Kampala*. https://thinkwell.global/wp-content/uploads/2022/07/13.-A-Profile-of-Women-Seeking-MCH-Services-in-Public-Facilities-in-Kampala.pdf (2022).
40. The Republic of Uganda - Ministry of Health. *Reproductive, Maternal, Newborn, Child, Adolescent and Healthy Aging Sharpened Plan for Uganda 2022/23–2027/28*. https://www.globalfinancingfacility.org/sites/default/files/Uganda-GFF-Investment-Case-2022-2027.pdf (2022).
41. Ministry of Health Uganda - Climate Change and Health. *Health - National Adaptation Plan (H-NAP) 2025 - 2030*. https://library.health.go.ug/sites/default/files/resources/UGANDA%20CLIMATE%20HNAP%202024_11zon_0.pdf (2024).
42. Ruel, M. T. & Alderman, H. Nutrition-sensitive interventions and programmes: how can they help to accelerate progress in improving maternal and child nutrition? *The Lancet* **382**, 536–551 (2013).
43. UNICEF. *UNICEF Nutrition Strategy 2020 -2030*. https://www.unicef.org/media/91741/file/UNICEF-Nutrition-Strategy-2020-2030-Brief.pdf (2020).
44. Ministry of Health Uganda. *SERVICE STANDARDS AND SERVICE DELIVERY STANDARDS FOR THE HEALTH SECTOR*. https://library.health.go.ug/sites/default/files/resources/Health%20Sector%20Service%20Standards%20%26%20Service%20Delivery%20Standards_2016.pdf (2016).
45. Maplecroft. Urbanisation and Climate Change Risks. *Verisk Maplecroft* https://www.maplecroft.com/insights/analysis/84-of-worlds-fastest-growing-cities-face-extreme-climate-change-risks/ (2018).

46. Vermeiren, K., Van Rompaey, A., Loopmans, M., Serwajja, E. & Mukwaya, P. Urban growth of Kampala, Uganda: Pattern analysis and scenario development. *Landscape and Urban Planning* **106**, 199–206 (2012).
47. Ssemugabo, C., Nalinya, S., Lubega, G. B., Ndejjo, R. & Musoke, D. Health Risks in Our Environment: Urban Slum Youth' Perspectives Using Photovoice in Kampala, Uganda. *Sustainability* **13**, 248 (2020).
48. Doherty, J. Filthy Flourishing: Para-Sites, Animal Infrastructure, and the Waste Frontier in Kampala. *Current Anthropology* **60**, S321–S332 (2019).
49. Nakyagaba, G. N., Lawhon, M., Lwasa, S., Silver, J. & Tumwine, F. Power, politics and a poo pump: Contestation over legitimacy, access and benefits of sanitation technology in Kampala. *Singapore Journal of Tropical Geography* **42**, 415–430 (2021).
50. Wilby, R. L. *et al.* Spatial and temporal scaling of sub-daily extreme rainfall for data sparse places. *Clim Dyn* **60**, 3577–3596 (2023).
51. Umer, Y., Jetten, V., Ettema, J. & Lombardo, L. Application of the WRF model rainfall product for the localized flood hazard modeling in a data-scarce environment. *Nat Hazards* **111**, 1813–1844 (2022).
52. Tweheyo, R. *et al.* 'Nobody is after you; it is your initiative to start work': a qualitative study of health workforce absenteeism in rural Uganda. *BMJ Glob Health* **2**, e000455 (2017).
53. Ministry of Health Uganda. *Uganda Hospital and Health Centre IV Census Survey*. http://library.health.go.ug/sites/default/files/resources/Uganda%20Hospital%20and%20health%20Centre%20IV%20Census%20Survey%202014.pdf (2014).
54. Uganda Bureau of Statistics. Uganda administrative boundaries. (2019).
55. Regional Centre for Mapping of Resource for Development. Uganda SRTM DEM 30 meters. https://opendata.rcmrd.org/datasets/0e2d5484fff84d9a8bb9e05173de61ca/about (2018).
56. Zanaga, D. *et al.* ESA WorldCover 10 m 2021 v200. Zenodo (2022).
57. OpenStreetMap contributors. Planet dump retrieved from https://planet.osm.org. (2017).

58. McClean, F., Walsh, C., Lwasa, S. & Ddumba, D. Modelled flood extents for Kampala, Uganda. NERC EDS Environmental Information Data Centre https://doi.org/10.5285/E53DEA2E-CB25-4F0F-B5F9-937EECF15AFF (2021).
59. Maina, J. *et al.* A spatial database of health facilities managed by the public health sector in sub Saharan Africa. *Scientific Data* **6**, 134–134 (2019).
60. Bondarenko, M., Kerr, D., Sorichetta, A., Tatem, A., & WorldPop,. Census/projection-disaggregated gridded population datasets, adjusted to match the corresponding UNPD 2020 estimates, for 51 countries across sub-Saharan Africa using building footprints. University of Southampton https://doi.org/10.5258/SOTON/WP00683 (2020).
61. Ray, N. & Ebener, S. AccessMod 3.0: computing geographic coverage and accessibility to health care services using anisotropic movement of patients. *International Journal of Health Geographics* **7**, 63–63 (2008).
62. WHO Department of Health Systems Governance and Financing. AccessMod 5. https://www.accessmod.org (2021).
63. Lubbers, R. RikLubbers/AMRemote_looped_MLC. (2024).
64. UNFPA. *IMPLEMENTATION MANUAL FOR DEVELOPING A NATIONAL NETWORK OF MATERNITY UNITS*. https://www.unfpa.org/sites/default/files/pub-pdf/2023%20EN_EmONC_web.pdf (2020).
65. Molenaar, L., Hierink, F., Brun, M., Monet, J.-P. & Ray, N. Travel scenario workshops for geographical accessibility modeling of health services: A transdisciplinary evaluation study. *Front. Public Health* **10**, (2023).
66. Watmough, G. R. *et al.* Using open-source data to construct 20 metre resolution maps of children's travel time to the nearest health facility. *Sci Data* **9**, 217 (2022).
67. Makanga, P. T. *et al.* Seasonal variation in geographical access to maternal health services in regions of southern Mozambique. *International Journal of Health Geographics* **16**, 1–16 (2017).

68. Tobler, W. Three Presentations on Geographical Analysis and Modeling: Non- Isotropic Geographic Modeling; Speculations on the Geometry of Geography; and Global Spatial Analysis (93-1). https://escholarship.org/uc/item/05r820mz (1993).
69. R Core Team. R: A Language and Environment for Statistical Computing. (2025).
70. Calvin, K. *et al. IPCC, 2023: Climate Change 2023: Synthesis Report. Contribution of Working Groups I, II and III to the Sixth Assessment Report of the Intergovernmental Panel on Climate Change [Core Writing Team, H. Lee and J. Romero (Eds.)]. IPCC, Geneva, Switzerland.* https://www.ipcc.ch/report/ar6/syr/ (2023) doi:10.59327/IPCC/AR6-9789291691647.
71. Blasini, A. W., Waiswa, P., Wanduru, P., Amutuhaire, L. & Moyer, C. A. 'Even when people live just across the road…they won't go': Community health worker perspectives on incentivized delays to under-five care-seeking in urban slums of Kampala, Uganda. *PLOS ONE* **16**, (2021).
72. Orderud, H., Härkönen, J., Hårsaker, C. T. & Bogren, M. Floods and maternal healthcare utilisation in Bangladesh. *Popul Environ* **44**, 193–225 (2022).
73. Wong, K. L. M., Brady, O. J., Campbell, O. M. R., Banke-Thomas, A. & Benova, L. Too poor or too far? Partitioning the variability of hospital-based childbirth by poverty and travel time in Kenya, Malawi, Nigeria and Tanzania. *Int J Equity Health* **19**, 15 (2020).
74. Lubbers, R. U., Waiswa-Goossens, T., Weitkamp, G. & Biesma, R. Geographical accessibility to public healthcare facilities and undernutrition in children under-5 in Uganda: a cross-sectional spatial analysis. *African Geographical Review* https://www.tandfonline.com/doi/abs/10.1080/19376812.2025.2538772 (2025).
75. Mallett, L. H. & Etzel, R. A. Flooding: what is the impact on pregnancy and child health? *Disasters* **42**, 432–458 (2018).
76. Petricola, S., Reinmuth, M., Lautenbach, S., Hatfield, C. & Zipf, A. Assessing road criticality and loss of healthcare accessibility during floods: the case of Cyclone Idai, Mozambique 2019. *International Journal of Health Geographics* **21**, 14 (2022).

77. Hierink, F., Rodrigues, N., Muñiz, M., Panciera, R. & Ray, N. Modelling geographical accessibility to support disaster response and rehabilitation of a healthcare system: an impact analysis of Cyclones Idai and Kenneth in Mozambique. *BMJ Open* **10**, e039138 (2020).
78. Chen, T., Radke, J., Lang, W., Li, X. & Li, X. Environment resilience and public health: Assessing healthcare's vulnerability to climate change in the San Francisco Bay Area. *Growth and Change* **51**, 607–625 (2020).
79. Coles, D., Yu, D., Wilby, R. L., Green, D. & Herring, Z. Beyond 'flood hotspots': Modelling emergency service accessibility during flooding in York, UK. *Journal of Hydrology* **546**, 419–436 (2017).
80. Zhou, X., Wang, S., Yao, S. & Fang, L. Influence of Urban Flooding on the Spatial Equity of Access to Emergency Medical Services Among Nursing Homes in Shanghai. *Land* **14**, 309 (2025).
81. Banke-Thomas, A., Wong, K. L. M., Ayomoh, F. I., Giwa-Ayedun, R. O. & Benova, L. "In cities, it's not far, but it takes long": comparing estimated and replicated travel times to reach life-saving obstetric care in Lagos, Nigeria. *BMJ Glob Health* **6**, e004318 (2021).
82. Ogega, O. M., Scoccimarro, E., Misiani, H. & Mbugua, J. Extreme climatic events to intensify over the Lake Victoria Basin under global warming. *Sci Rep* **13**, 9729 (2023).
83. Pietroiusti, R. *et al.* Possible role of anthropogenic climate change in the record-breaking 2020 Lake Victoria levels and floods. *Earth System Dynamics* **15**, 225–264 (2024).
84. World Bank. *CLIMATE RISK COUNTRY PROFILE - Uganda*. https://climateknowledgeportal.worldbank.org/sites/default/files/2021-05/15464-WB_Uganda%20Country%20Profile-WEB%20%281%29.pdf (2021).
85. Soman, S., Beukes, A., Nederhood, C., Marchio, N. & Bettencourt, L. M. A. Worldwide Detection of Informal Settlements via Topological Analysis of Crowdsourced Digital Maps. *ISPRS International Journal of Geo-Information* **9**, 685 (2020).
86. Fischer, S. & Schumann, A. H. Opportunities and Limitations of Specifying Flood Types. in *Type-Based Flood Statistics: An Interlink Between Stochastic and Deterministic Flood Hydrology*

(eds. Fischer, S. & Schumann, A. H.) 43–49 (Springer International Publishing, Cham, 2023). doi:10.1007/978-3-031-32711-7_4.

87. Piadeh, F., Behzadian, K. & Alani, A. M. A critical review of real-time modelling of flood forecasting in urban drainage systems. *Journal of Hydrology* **607**, 127476 (2022).
88. Kumar, V., Sharma, K. V., Caloiero, T., Mehta, D. J. & Singh, K. Comprehensive Overview of Flood Modeling Approaches: A Review of Recent Advances. *Hydrology* **10**, 141 (2023).
89. Banke-Thomas, A. *et al.* Geographical accessibility to functional emergency obstetric care facilities in urban Nigeria using closer-to-reality travel time estimates: a population-based spatial analysis. *The Lancet Global Health* **12**, e848–e858 (2024).
90. Cuervo, L. G. *et al.* Dynamic accessibility by car to tertiary care emergency services in Cali, Colombia, in 2020: cross-sectional equity analyses using travel time big data from a Google API. *BMJ Open* **12**, e062178 (2022).
91. Macharia, P. M. *et al.* A geospatial database of close-to-reality travel times to obstetric emergency care in 15 Nigerian conurbations. *Sci Data* **10**, 736 (2023).

Supplementary Files

This is a list of supplementary files associated with this preprint. Click to download.

- SupplementaryTable1.docx
- SupplementaryMethods1.docx
- SupplementaryMethods2.docx
- Supfig1mergedlandcoverswfloods.pdf
- SupFig2indexcomparison.pdf